Nano Energy 124 (2024) 109460

Contents lists available at ScienceDirect

Nano Energy

journal homepage: www.elsevier.com/locate/nanoen

Full paper

Variable capacity polymer based energy harvesters with integrated macroporous elastomer springs

Qixiang Jiang [a], Veronika Otáhalová [a,b], Victor Burré [a], Hannah S. Leese [c], Milo S.P. Shaffer [d], Robert Hahn [e], Angelika Menner [a,*], Alexander Bismarck [a,f,**]

[a] Polymer & Composite Engineering (PaCE) Group, Institute of Materials Chemistry & Research, Faculty of Chemistry, University of Vienna, Währingerstr. 42, A-1090, Vienna, Austria
[b] Sigma Clermont, CS20265 - Campus des Cézeaux, 27 Rue Roche Genès, Aubière 63178, France
[c] Department of Chemical Engineering, University of Bath, Claverton Down, Bath BA2 7AY, UK
[d] Nanostructured Hierarchical Assemblies and Composites (NanoHAC) group, Department of Chemistry, Imperial College London, South Kensington Campus, London SW7 2AZ, UK
[e] Institute for Reliability and Microintegration (IZM) Fraunhofer, Argelsrieder Feld 6, Weßling 82234, Germany
[f] Department of Chemical Engineering, Imperial College London, South Kensington Campus, London SW7 2AZ, UK

ARTICLE INFO

Keywords:
Variable capacity energy harvester
Spring element
Elastomers
Macroporous polymers
Emulsion templating

ABSTRACT

We introduce a manufacturing concept of variable capacity energy harvesters consisting of macroporous springs integrated within a conducting silicone rubber and dielectric. Printing and polymerising emulsion templates resulted in macroporous spring elements, which were coated with conducting silicone rubber to maintain the active contact surface. By increasing size and number of these springs, the capacitance change of the energy harvesters during compression and recovery increased from 0.4 nF/cm^2 to 0.8 nF/cm^2. During cyclic loading with 30 N at 2 Hz, the energy harvesters with macroporous springs delivered a power density of 0.58 μW/cm^2 at a bias voltage of 50 V, which was 25 times higher than the control without springs. The energy harvesters provided a constant power output over three hours of cyclic loading (21,600 cycles), indicating their structural stability and the durability of the macroporous springs.

Introduction

Portable and wearable (flexible) electronic devices offer new possibilities to satisfy people's needs for medical and health monitoring, as well as opportunities in entertainment and communication applications. However, such portable devices require electrical energy. The conventional solution of replacing (or recharging rechargeable) batteries does not readily permit continuous service. Portable energy harvesters provide an alternative: they can scavenge and convert ambient energy sources, such as human motion, into electrical power, which can be used to charge portable batteries or power portable devices, continuously.

Energy harvesters can convert mechanical energy into electric power using piezoelectric [1], electromagnetic [2] and electrostatic [3] effects or a combination thereof [4]. Electrostatic energy harvesters exploiting variable capacitance [5] offer numerous advantages, including simple construction, straightforward down-scale, and the potential to use low-cost materials. A simple model of a variable capacitor harvester comprises two electrodes isolated by air or a dielectric [6]. The harvesters are charged by a bias voltage. Upon oscillating movement between the electrode and dielectric the capacitance of the device changes, causing charges to flow through the external circuit; the energy converted from mechanical oscillation can be used by the electrical load [7,8]. As such, the performance of the electrostatic energy harvesters increases with increasing bias voltage, capacitance change and frequency [9]. However, practical variable capacitor harvesters based on this model are usually based on a rigid structure [10], which is limiting in many contexts, for example in wearable devices. Harvesters based on reverse electrowetting of liquid electrodes on dielectrics (REWOD) have been disclosed [11,12]; they exploit the high reversibility and smooth contact of liquid metal droplets on the dielectric, which covers a counter

* Corresponding author.
** Corresponding author at: Polymer & Composite Engineering (PaCE) Group, Institute of Materials Chemistry & Research, Faculty of Chemistry, University of Vienna, Währingerstr. 42, Vienna A-1090, Austria.
E-mail addresses: angelika.menner@univie.ac.at (A. Menner), alexander.bismarck@univie.ac.at (A. Bismarck).

https://doi.org/10.1016/j.nanoen.2024.109460
Received 2 January 2024; Received in revised form 21 February 2024; Accepted 4 March 2024
Available online 6 March 2024

electrode. The liquid metal droplets are deformed or can be moved to change the contact or overlap area with the dielectric, causing a change of the capacitance of the REWOD harvesters. They have been shown to be particularly effective for scavenging mechanical energy from low frequency motions, e.g. rolling or stepping, into electrical energy. However, such energy harvesters need room temperature liquid metal electrodes; there are only two options, both of which are problematic. Mercury has high toxicity, while Galinstan and related alloys need to be encapsulated completely to avoid oxidation, making the REWOD design difficult to adapt for practical implementations [13,14]. Moon et al. [15] adapted the design of REWOD harvesters. They use water droplets that bridge two conducting plates, exploiting the formation of electrical double layers (EDL) at the water/plate interface. When the water bridge is mechanically modulated, the contact area and capacitance of EDL changes. The charges can be carried by ions in the water and the counter charges flow through an external load. This design of REWOD energy harvesters does not require an external bias and the liquids in the harvester are only low-toxic electrolytes, e.g. aqueous solutions of salts [16], ionic liquids [17] or swollen hydrogels [18]. Despite the beauty of such harvesters containing a liquid bridge, such harvester concepts have only been tested in laboratory scale, e.g. testing on a shaker [19] with all liquid droplets sitting on a horizontal plate [15]; production of practical REWOD energy harvester devices is still challenging.

Alternatively, variable capacitance in energy harvesters can be modulated by the variable contact between flexible conductive electrodes and dielectric. Such energy harvesters are also suitable for scavenging energy from low frequency motions [13]. Furthermore, the inherent mechanical properties of the materials and structure allow the harvesters to be easily incorporated into fabrics or shoes without reducing wearing comfort. The first development of dielectric elastomers for harvesters was disclosed by Pelrine et al. in 2001 [20]; thereafter, successful applications of harvesters containing dielectric elastomers in wearable devices [21] and as artificial muscles [22] have been demonstrated. Flexible electrodes consisting of an elastomeric substrate and a conductive surface (e.g. coated with carbon powder) have been developed for energy harvesters [23]; the electrodes can be designed to be largely stretchable without losing electric conductivity [24]. Hahn et al. [13] prepared variable capacitor energy harvesters containing silicone rubber-based electrodes and dielectric coated flexible substrate. The cyclic compression of their electrodes on a dielectric surface generated a power of up to 1.5 $\mu W/cm^2$. However, they identified the issue that the adhesion between the flexible electrode and the rigid dielectric can reduce detaching speed, which reduced energy harvesting efficiency. One solution is to incorporate spring elements to help the variable capacitors recover to their original state after each loading cycle. Many electrostatic energy harvester prototypes contain coil springs [25,26]. The shape of the springs makes them difficult to scale down and adapt for wearable devices and reduces the volumetric energy density of the harvesters. In flexible energy harvesters, elastomeric cubic or cylindrical spring or spacer elements have been installed between the flat electrode and dielectric [27,28]. During loading the springs are compressed, allowing contact between the electrodes and dielectric; on unloading, the springs recover to their original shape, detaching the electrode from the dielectric. As compared to coil springs, the elastomer springs save considerable space in the energy harvester, yet they still occupy some of the active surface of dielectric, limiting the maximum energy output. In addition, to maximise efficiency, the mechanical properties of the springs need to be well-defined to ensure intimate electrode-dielectric contact at low loads, as well as rapid recovery with low hysteresis. Elastomeric foams are promising candidate spring elements for energy harvesters, given their fast shape-recovery and adjustable mechanical properties. However, so far, foam springs have only been used in large harvesters [29,30]. Downscaling foam springs to fit in micro-sized energy harvesters has yet to be reported. This omission could be due to the fact that the foam springs are typically fabricated by machining solid foam products.

Emulsion templating has been widely used to produce macroporous polymers [31]. Typically, an emulsion is prepared with monomers in the continuous phase and liquid droplets as the dispersed templating phase; polymerisation of the monomers and removal of the templating phase produces macroporous polymers, whose porosity and morphology are replicate of the volume and geometry of the liquid droplets. The mechanical properties of the emulsion templated macroporous polymers can be tailored by the choice of monomers and the proportions of the emulsion phases. If the volume fraction of the discontinuous emulsion phase is sufficiently high that the droplets are forced into contact, the system is termed a high internal phase emulsion (HIPE); once polymerised, the resulting "polyHIPEs" have low densities and can form open-celled foams. A key advantage of this templating approach is the fluidity of the emulsions, which can be moulded or printed to create macroporous polymers with desired shapes after curing. In previous work, we demonstrated the use of polyurethane diacrylate (PUDA) and ethylhexyl acrylate (EHA) based HIPEs as inks [14]. The printing and subsequent polymerisation of the inks resulted in macroporous polyHIPE cages with a wall thickness of approximately 2 mm. These polymer cages were used as spring elements for reverse electrowetting on dielectric energy harvesters, assisting the deformation and recovery of the liquid electrodes in the harvesters.

In this work, we will introduce a concept to realise capacitive energy harvesters with integrated macroporous polymer springs; the energy harvesters can convert energy from cyclical mechanical compression (e.g. energy from jogging) into electrical energy. The electrodes, dielectrics and the spring elements, namely the emulsion templated macroporous elastomers, were produced from liquid starting materials, allowing a sequenced layer by layer deposition. The performance of the harvesters with and without a spring element was investigated under a cyclic compression simulating jogging conditions to assess the effectiveness of the integrated springs.

Experimental section

Materials

Copper coated polyimide (Kapton®) films with a total thickness of 100 μm were kindly provided by Eurecat (Barcelona, Spain). Ethylhexyl acrylate (EHA), strontium doped barium titanate (SBTO) nanopowder (average particle size < 100 nm) and $CaCl_2{\cdot}2\ H_2O$ were purchased from Sigma-Aldrich. Polyurethane diacrylate Ebecryl 8402 (PUDA) was kindly supplied by Cytec (Diegem, Belgium), the surfactant Hypermer B246 by Croda (East Yorkshire, UK), the photoinitiator 2-hydroxy-2-methyl-1-phenyl-1-propanone (Darocur 1173) by BTC Europe GmbH (Düsseldorf, Germany) and the 2-component conducting silicone rubber (Elastosil LR3162 A/B) by Wacker (Stuttgart, Germany). Prime™ 20ULV epoxy with a slow (ULV) hardener was purchased from Gurit (Newport, UK). All chemicals were used as received.

Preparation of emulsion templates

The equipment for preparing emulsion templates consisted of a glass reaction vessel equipped with a dropping funnel and an anchor stirrer connected to an overhead stirrer. The continuous HIPE phase was prepared by mixing 36 vol% PUDA, 60 vol% EHA and 3 vol% Hypermer B246 in the vessel; 2 mol% (with respect to the double bonds in the monomers) Darocur 1173 was added into the mixture. An aqueous solution of 10 g/L $CaCl_2{\bullet}2\ H_2O$ was dropped into the continuous phase while stirring at a speed of 400 rpm to reach an internal phase volume ratio of 75% (with respect to the volume of the emulsion). Afterwards, the HIPE was stirred at a speed of 2000 rpm for 2 min to obtain a homogeneous emulsion.

Production of polyHIPE springs

3 cm × 10 cm copper polyimide Kapton® films, which were etched (by Eurecat, Barcelona, Spain) to have two 2 mm wide and 10 cm long copper lines, were used as the substrates (Scheme 1a, Step 1). The HIPEs were syringe printed using a home-built syringe printing system consisting of a universal CNC model-making machine (Stepcraft 420, Stepcraft GmbH, Iserlohn, Germany) equipped with a syringe dispenser (EFD Ultra 2800, Nordson, Oberhaching, Germany). A needle with an inner diameter of 200 μm and an outer diameter of 420 μm was used for

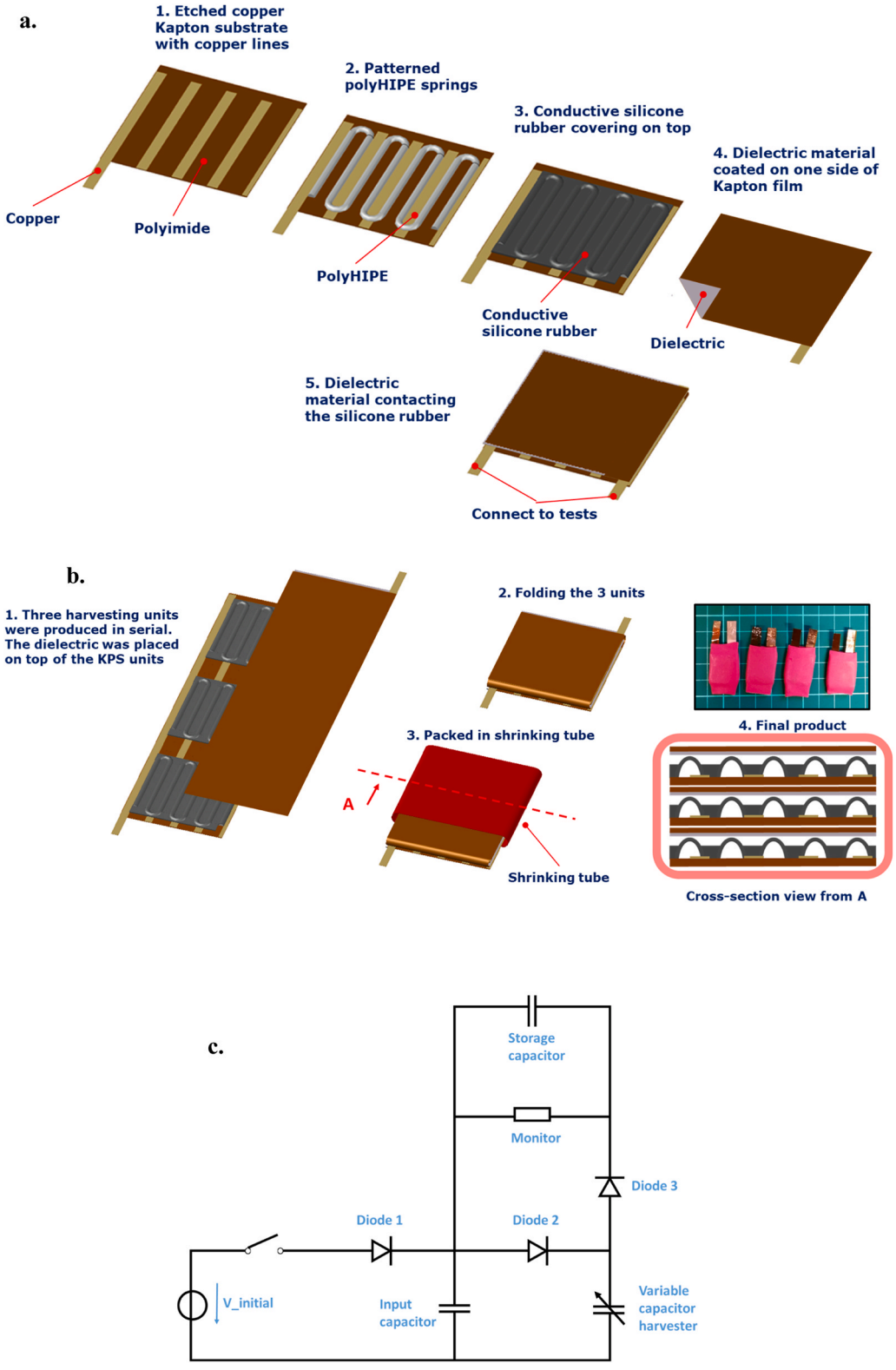

Scheme 1. Layer-by-layer deposition of polyHIPE as springs and conductive silicone rubber as electrodes on etched Kapton® films for production of an energy harvesting unit (a). Production of demonstration energy harvesters (b). Energy harvesting performance of the harvesters was tested using a harvester meter with a circuit diagram shown in (c).

syringe printing. The distance d between the needle and the substrate was 200 μm, 300 μm and 400 μm, respectively, which determined the target height of the printed HIPEs. The printing speed S was 5 mm/s; the dispensing rate α was calculated as follows:

$$\alpha = \pi(d/2)^2 \bullet S \quad (1)$$

The HIPE was printed into 14 parallel meandering lines (Scheme 1a, Step 2), the distance between each line was set to be 0.75 mm, 1 mm and 1.5 mm, respectively. The printed HIPE micropatterns were placed in a water bath and UV polymerised for 2 min using handheld UV lamp (UVP-B100AP, UVP, UK) with a wavelength of 365 nm; the UV lamp was placed ~10 cm above the printed HIPE. The polymerised polyHIPE springs were dried in an oven at 70 °C.

Fabrication of conducting silicone rubber electrodes

The two components of the conducting silicone rubber were mixed in a weight ratio of 1:1. The resulting paste was manually cast on the Kapton® foil decorated with the polyHIPE springs (Scheme 1a, Step 3) using a stainless-steel casting blade. The casting gap was set to be smaller than the height of the polyHIPE springs (Table 1). Afterwards, the silicone paste was cured in an oven at 100 °C for 20 min. The parameter set used for the fabrication of K(apton)-P(olyHIPE)-S(ilicone) units are listed in Table 1. The area of the KPS units was ca. 2 cm^2, 3 cm^2 and 4 cm^2 for spring distance of 0.75 mm, 1 mm and 1.5 mm, respectively, in order to keep the number of spring elements within the unit constant. The exact area of KPS units was measured by ImageJ.

Preparation of dielectric

The dielectric (Scheme 1a, Step 4) was prepared as reported by Leese et al. [32]. Briefly, SBTO powder was sonicated in acetone for 30 min in an ultrasonication bath (USC300T, 80 W). The suspension was mixed with epoxy (Prime 20ULV, Gurit) to disperse 20 wt% SBTO in epoxy by vigorous overhead stirring. The acetone was driven off in a vacuum oven and the mixture fully degassed. Prior to screen printing, a (a slow ULV) hardener with a concentration of 23 wt% with respect to the epoxy was mixed into the SBTO-epoxy suspension. This mixture was degassed for 30 min. The inks were printed using a flat screen printer (ATMA AT-80 P/B, ATMA, Taiwan) equipped with a 110 T polyester screen mesh. The distance between the screen and substrate (copper Kapton® film) was fixed at 3 mm. The average thickness of the dielectric films was 10 μm. The printed dielectric was cured at 100°C for 5 h.

Preparation of demonstration energy harvesters

Demonstration energy harvesters were produced by using the architecture of KPS5 and KPS7 (Table 1). Three patches of KPS 5 or 7 were printed onto a single Kapton® film followed by UV polymerisation of the HIPEs and drying of the polyHIPEs. The conductive silicone rubber paste was applied over the polyHIPE springs to form three KPS units connected in series (Scheme 1b, Step 1, photos of each step for production of three KPS units on Kapton film is shown in Figure S1, ESI). Each KPS unit had an area of 1.4 cm × 1.4 cm. The KPS units were covered with the dielectric film. The resulting structures were folded and sealed in heat shrink tubing to produce demonstration energy harvesters (Scheme 1b, Step 2 and 3). To produce a control harvester, three patches of conductive silicone rubber (1.4 cm × 1.4 cm) were cast and cured on a copper Kapton film without polyHIPE springs. The copper Kapton® film with three patches of silicone rubber of a thickness of 120 μm was folded along with the dielectric film and packed in a shrink tube.

Table 1
Processing parameters set used for production of KPS units.

	Distance between the needle and the substrate when printing HIPEs, d (μm)	Distance between two printed HIPE lines, D (mm)	Casting gap size when casting the silicone rubber (μm)
KPS1	200	1.5	140
KPS2	200	1	140
KPS3	200	0.75	140
KPS4	300	1.5	190
KPS5	300	1	190
KPS6	400	1.5	330
KPS7	400	1	330

Characterisation of KPS units and demonstration energy harvesters

Morphology of KPS units

was investigated using scanning electron microscopy (SEM, JCM-6000, JEOL GmbH, Eching, Germany). The cross-section, of the samples, cut by scalpel, was gold coated (JFC-1200, JEOL GmbH, Eching, Germany) prior to imaging. The SEM images were further analysed using ImageJ to determine the height of the polyHIPE springs, the distance between neighbouring springs and the thickness of the conducting silicone rubber coating.

Capacitance change during compression

The KPS units were compressed against a dielectric coated films using a universal mechanical testing machine (Instron 3345, Instron GmbH, Buckinghamshire, UK) equipped with a 500 N load cell. The samples were compressed to reach a stress of 0.15 MPa at a speed of 0.5 mm/min. Afterwards, the applied load was reduced to zero within 1 s and the sample allowed to recover to a load-free state. The capacitance of the harvesting units was monitored during the compression cycle using a voltammeter (Voltcraft VC940) in capacitance mode. The normalised capacitance (by area of the KPS units) of the units as a function of stress was recorded. The normalised capacitance change was defined by the difference between the normalised capacitance of the harvesters in the loaded and unloaded state. The cyclic capacitance change of demonstration energy harvesters were tested by compressing the energy harvesters from 0 to 50 N for 100 cycles using a universal mechanical testing machine (Instron 5969, Instron GmbH, Buckinghamshire, UK) equipped with a 1 kN load cell; the capacitance change was monitored using the voltammeter and normalised by the area of three KPS units in the energy harvesters.

Energy harvesting tests

were carried out by monitoring the voltage accumulation or current flow of a demonstration energy harvester during a cyclic compression. The energy was measured using a home-built energy harvesting meter (Scheme 1c) provided by IZM Fraunhofer (Berlin, Germany); the principle of the harvester has been reported in the literature [13, [33]). Briefly, before testing a bias of 50 V was stored on the input capacitor (1 μF, thus providing an initial energy of 2.5 mJ), which was used to charge the variable capacitor harvester. Upon the decrease of the capacitance of the harvester, its voltage increased, the charges flow to the storage capacitor, e.g. charge quantity reduced while voltage is constant. When the capacitance of the harvester increased, its voltage decreased, allowing re-charge of the harvester from the initial capacitor. The cyclic loading of the harvester was realised using a dynamic mechanical analyser (DMA, RSAG2, TA Instrument, Eschborn, Germany). The harvesters were loaded in compression from 0 to 30 N at a frequency of 2 Hz for 10 min to accumulate charges on a storage capacitor of 1 μF; the voltage on the storage capacitor was monitored using the harvesting meter. Subsequently the storage capacitor was short-circuited through a 1 MΩ resistor to release all charges. The charging procedure was repeated 15 times. The energy E in the storage capacitor was calculated:

$$E = \frac{1}{2} \bullet C \bullet U^2 \quad (2)$$

where C is the capacitance of the storage capacitor, which was 1 μF, and U the voltage in the storage capacitor. The power density of the energy harvester was calculated by the energy on the storage capacitor over time over area of KPS. To confirm a stable energy output the storage capacitor was short-circuited through a 2 MΩ resistor. The harvesters were cyclically loaded for 3 h while monitoring the current flow; the current was recorded as a function of time.

Results and discussion

Copper coated Kapton® films were used as substrates for the KPS units. Prior to the deposition of the polyHIPE spring elements and conductive silicone rubbers, the Kapton films were etched to expose the polyimide surface and improve the adhesion of the spring units, while leaving copper lines as conductive wires. The highly conductive copper tracks (5.8×10^7 S/m) are needed for low loss current collection from the whole device; however, the less conductive, conducting silicone rubber layer (9.1 S/m) is sufficient to transfer the current locally. More optimised patterns for the copper current collector could be designed quantitatively in future [34]. The PUDA and EHA based emulsion templates were formulated as previously reported [14]. The viscous but liquid emulsions were syringe printed in a snake pattern onto the Kapton films (Scheme 1a). Fig. 1 shows SEM images of cross-sections of two KPS units. The distance between neighbouring springs, defined by the distance from the centre line of one spring to that of the neighbouring one, corresponded to the set distance between the printed emulsion lines. The cross-section of the polyHIPEs has the shape of a wetting cylinder (Fig. 1a-c); the height of the springs was lower than the height of the printed emulsion lines (Table 1 and Table 2) because the HIPEs partially wet the Kapton® films. The spreading motion of the printed emulsion was arrested by the high zero shear viscosity of the HIPE template [35]. After polymerisation of the emulsion template, the polyHIPEs have an interconnected pore structure (Fig. 1d), which is typical for polyHIPEs produced from surfactant-stabilised HIPEs [36]. The polyHIPE springs were covered completely by the conducting silicone rubber (Fig. 1a-c), allowing maximum active contact area of the variable capacitive energy harvesters. Furthermore, the wavy surface of the silicone rubber, caused by the wetting cylinder shape of the polyHIPE springs and the flat surface of the Kapton film, enabled the polyHIPE springs to function (Fig. 1a, b). Due to the wavy electrode surface, this conductive silicon rubber electrode can be compressed towards the dielectric counterpart by between 50 μm and 75 μm, depending on the design used (Tables 1 and 2). Since the geometry of the springs controls the relative contact area and the electrode-dielectric separation during cycling, a range of design parameters was tested (Table 1). These values were chosen to balance compliance of the device and relative contact / separation area between the electrode and dielectric.

Table 2
The size of the polyHIPE lines, pitches and silicone rubber in KPS units.

	Actual height of polyHIPE springs (μm)	Distance between neighbouring polyHIPE springs, D (mm)	Thickness of silicone rubber coating (μm)
KPS1	104 ± 20	1.5	62 ± 11
KPS2	116 ± 4	1	62 ± 12
KPS3	120 ± 19	0.75	62 ± 9
KPS4	198 ± 15	1.5	126 ± 17
KPS5	180 ± 14	1	114 ± 14
KPS6	330 ± 14	1.5	230 ± 11
KPS7	319 ± 18	1	268 ± 18

Once the KPS units were combined with the dielectric counterpart, they were compressed using a universal mechanical tester (Video SI 1,

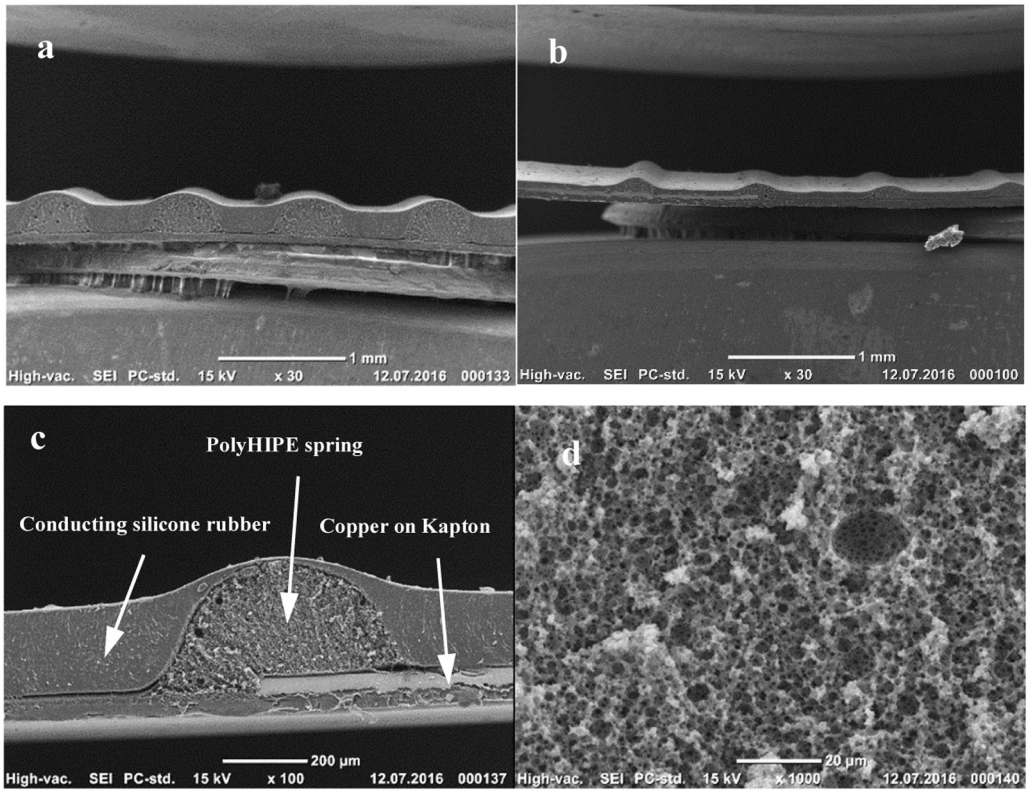

Fig. 1. Characteristic SEM images of cross-sections of KPS units with a distance in between polyHIPE springs of 1 mm and with a spring height of 300 μm (a) and 120 μm (b). The cross-section of KPS unit shows the Kapton film with a copper strip, polyHIPE spring and conducting silicone rubber (c). The polyHIPE springs have an interconnected porous structure (d).

plane harvester, Video SI 2 with integrated springs), while recording the capacitance as function of stress. With increasing stress the polyHIPE springs were compressed, allowing for the contact area between the conducting silicone rubber and the dielectric to increase, resulting in an increased capacitance of the harvester (Fig. 2). Upon removal of the applied load the springs recovered, pushing the dielectric away from the silicone rubber electrode, thus minimising the contact area resulting in the capacitance to drop back to the original value (shown as recovery in Fig. 2). Bringing the electrodes closer together (in this case the conductive silicone, and the copper substrate supporting the SBTO dielectric) increases capacitance inversely proportionally to the distance between them. In addition, the better the contact between the electrode and the dielectric, the higher the effective dielectric constant of the capacitor. In this system, removing the low dielectric constant air gap is likely the critical factor; this effect is also the motivation for using a high dielectric constant SBTO composite coating (dielectric constant of 18) [37] to maximise the capacitance variation between the two states.

The theoretical capacitance change of harvesters containing KPS units comprising 14 polyHIPE springs with a length l of 25 mm and dielectric during compression was calculated, making the following assumptions: 1) the polyHIPE springs have half cylinder shapes; 2) the silicone rubber formed a very thin layer covering the polyHIPE spring elements and the Kapton substrate and did not affect their stiffness; 3) during the compression of KPS units against the dielectric, the dielectric did not deform. The later assumption is justified since the printed SBTO thermoset composite dielectric has a much higher elastic modulus E (~2 GPa) compared to the polyHIPEs (270 kPa). The width t of the contact area between one spring / silicone rubber and the dielectric was calculated using the procedure proposed for compression of cylinders on a hard surface*:

$$t = n \bullet \sqrt{2 \bullet w \bullet r \bullet \left(\frac{1-\mu_1^2}{E_1} + \frac{1-\mu_2^2}{E_2}\right)} \tag{3}$$

where n is a constant, here n = 1.6, w the linear force, which is $w = \sigma \bullet D$, with σ being the applied stress, r the radius of the cylinder, which is equal to $\frac{d}{\sqrt{2}}$, E_1 and μ_1 elastic modulus and Poisson's ratio of the polyHIPE spring and E_2 and μ_2 the elastic modulus and Poisson's ratio of the dielectric. Here, we assumed the Poisson's ratio of the highly porous polyHIPE spring to be neglectable and the modulus of dielectric is close to infinite. Using these assumptions Eq. 3 simplifies to:

$$t = n \bullet \sqrt{2 \bullet w \bullet r \bullet \frac{1}{E_1}} \tag{4}$$

The contact area between the KPS units and dielectric and normalised capacitance as function of applied stress (on the entire KPS units, not only on the springs) can be calculated using:

$$C = \frac{t \bullet 14 \bullet l \bullet C_s}{D \bullet 14 \bullet l} \tag{5}$$

where C_s is 0.85 nF/cm^2 [13], (and 14 the number of springs separated by distance D in the harvester unit). We plotted the capacitance change as function of stress within a applied force range of 0 – 45 N. The normalised capacitance change increased with number (i.e. inverse of the distance D between two polyHIPE springs) and size of polyHIPE springs in the KPS unit; the relationship can be calculated by combining Eqs. 4 and 5:

$$C = n \bullet \sqrt{\frac{2 \bullet r \bullet \sigma}{E_1 \bullet D}} \tag{6}$$

For a given applied stress, the normalised capacitance is proportional to $\sqrt{r}/\sqrt{D}$. Increasing the number and size of the polyHIPE springs increases the overall stiffness of the KPS unit but also the available conductive silicone rubber contact area, which allowed for a large variable capacitance during compression.

Experimental data showed the capacitance of KPS units and dielectric increased during compression (Fig. 2) due to the increasing contact area (see Video SI 2); the measured capacitance increase agreed fairly well with the predicted capacitance (the comparison between the experimental and theoretical data is shown in S4, ESI). The distance between polyHIPE springs in KPS1–3 was 1.5, 1, and 0.75 mm, which did not significantly affect capacitance change with applied stress. The difference between the experimental and theoretical curves of these three KPS units can be explained by the insignificant influence of the number of spring elements present in a KPS unit when their size is rather small (i.e. polymerised from HIPEs that were printed with d = 200 μm). Furthermore, the experimental curves were lower than the calculated ones (S4, ESI). One possible explanation is the modulus of silicone rubber requiring higher stress to be compressed but this we neglected in our calculations. With increasing height of the printed polyHIPE springs (Table 2), the capacitance change of harvester units increased from 0.39 ± 0.04 nF/cm^2 (KPS1–3) to 0.72 ± 0.10 nF/cm^2 (KPS6–7) at an applied stress of 0.15 MPa (Fig. 3). This finding agreed with the predicted capacitance changes, which agreed better with the experimental data of the KPS units containing larger polyHIPE spring elements (e.g. KPS6–7, S4, ESI). Increasing the height of the polyHIPE springs, for a given spacing, has several effects. One is that the air gap between the silicone electrode and the dielectric surface increases, creating a greater change when the surfaces are brought into contact. Secondly, the proportions of the two components changes; since the polyHIPE has lower modulus (tensile modulus of 0.46 MPa, see section S2, ESI) than the dense conducting silicone rubber (tensile modulus of ~ 50 MPa; please note only that only the tensile modulus was reported and thus we compared those.), the average modulus of the structure is decreased. Thus, these springs (KPS 6–7) undergo a larger deformation when compared to those containing a smaller polyHIPE volumes (KPS 1–3), leading to a larger capacitance change as well as better agreement with the predicted curves. Increasing the applied compressive load even further resulted in higher capacitance changes (for KPS 7–0.93 ± 0.10 nF/cm^2 (Figure S2, ESI)) caused by pressing the dielectric further into the silicone rubber electrode (see Fig. 1c). However, the contact area between the silicone rubber coated on the Kapton films (i.e. between two polyHIPE springs) and the dielectric was not considered in our simple model (finite element modelling is required). Decreasing the distance between the neighbouring polyHIPE springs, corresponding to an increasing number of polyHIPE springs per KPS unit, had a more pronounced influence on the capacitance change of KPS4–5 and 6–7. Incorporating more spring elements into the KPS units increases the available interface area between conductive silicone rubber and dielectric but also decreases the overall stiffness of the KPS units (less stiff rubber is present in the device) promoting contact between electrode and dielectric in compression.

To build variable capacitance energy harvester demonstrators, the architecture of KPS units was screened by comparing the capacitance change normalised by volume: in other words, the capacitance change normalised by geometric electrode area (data shown in Fig. 3) divided by the total thickness of KPS unit and dielectric film, i.e. sum of thickness of copper Kapton® film (70 μm), polyHIPE springs (Table 2) and the Kapton® with the dielectric (100 μm). KPS5 and KPS7 had a capacitance change per volume of and 17.4 nF/cm^3 and 16.3 nF/cm^3, respectively, which were higher than that of KPS3 (13.8 nF/cm^3). Therefore, the KPS5 and KPS7 architectures were selected to manufacture demonstration energy harvesters. The demonstration energy harvesters contained three KPS units connected in series covered by dielectric and sealed in shrink tubing (Scheme 1b).

The capacitance change of the demonstrator harvester devices

[1] AA-SB-001Abbott Aerospace Link in: https://www.abbottaerospace.com/aa-sb-001/12-joints/12–3-general-treatment-of-contact-stresses/12–3-1-formulas-for-stress-and-deformations-due-to-pressure-between-elastic-bodies/

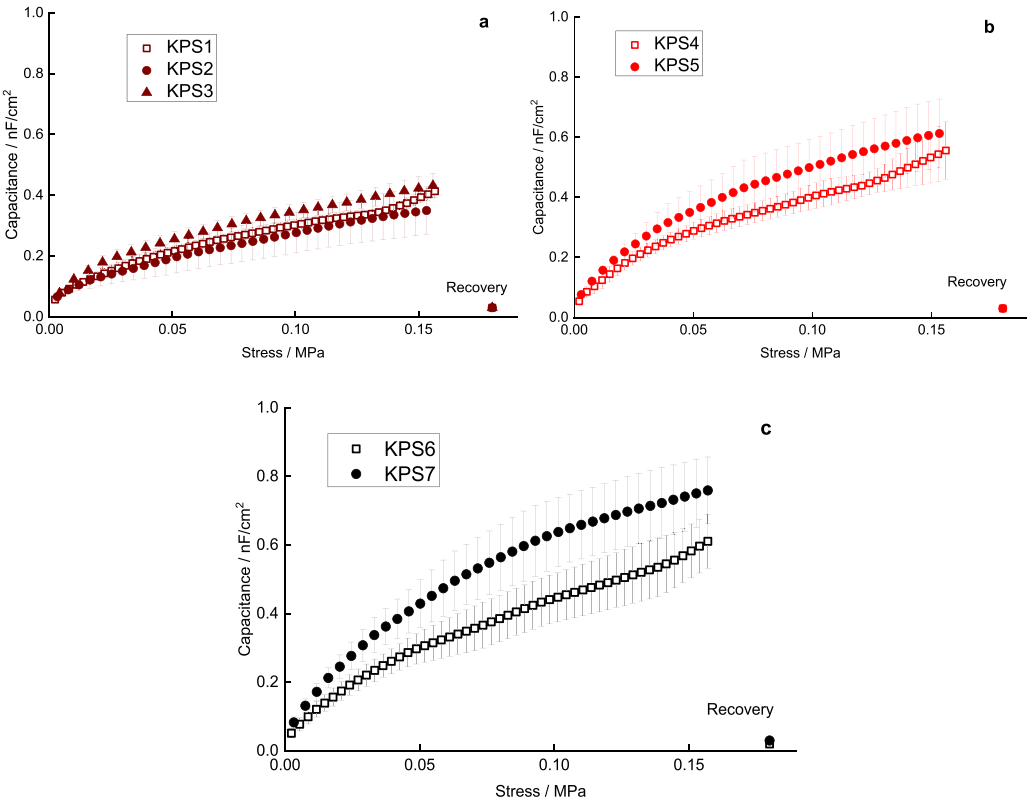

Fig. 2. Capacitance as a function of stress during compression of KPS units on a dielectric; the capacitance change is calculated as the capacitance at the device's most compressed stage (highest stress) minus the capacitance at recovery.

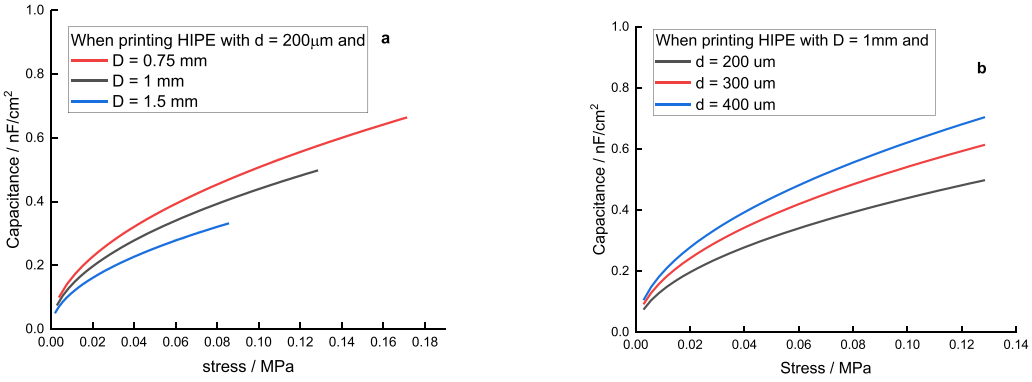

Fig. 3. Calculated normalised capacitance as function of applied stress to KPS units compressed against dielectric (a) with increasing number of incorporated polyHIPE springs, i.e. when printing the HIPE with a distance between two HIPE lines *D* of 1.5, 1, and 0.75 mm and (b) with increasing polyHIPE spring height, i.e. when printing the HIPE with needle to substrate distance *d* of 200, 300, and 400 μm.

containing either KPS or control harvester units, i.e. not containing any polyHIPE springs, were tested under a cyclic load up to 50 N. The capacitance at full loading and unloading of each cycle were recorded and normalised by geometric footprint area of the device (Fig. 4). Both energy harvester demonstrators containing polyHIPE springs had an initial capacitance of 0.100 ± 0.002 nF/cm^2, whereas the demonstrator containing control harvester units had a much higher average capacitance 0.20 ± 0.02 nF/cm^2 in the unloaded state. The presence of the polyHIPE springs in the flexible silicone rubber layer minimised the initial contact area between the flexible electrodes and dielectric as compared to the pure silicone rubber electrode, which was only separated from the dielectric by the surface roughness produced during manufacturing. The demonstrator harvesters containing KPS7 and KPS5 architectures also had higher capacitances under 50 N load (0.53 ± 0.01 nF/cm^2 and 0.49 ± 0.01 nF/cm^2, respectively) compared to the control harvester achieving a maximum a capacitance of 0.39 ± 0.01 nF/cm^2 (Fig. 3). This difference in capacitance was due to the more flexible architecture of silicone rubber layer supported on low stiffness polyHIPE springs, which increased contact between the silicone rubber and the dielectric at a given load. Furthermore, in the unloaded state, KPS5 and 7 had a constant capacitance for 100 cycles, indicating the robustness of the structure, while the capacitance of control harvester increased slightly but continuously, which could be due to a gradually increased adhesion between the conducting silicone rubber and the composite dielectric during cyclic compression. The demonstrator based on KPS7 had a higher capacitance under load than the one based on KPS5, consistent with the results shown in Fig. 2b and c. Overall, the use of polyHIPE springs increased the normalised capacitance change of the harvesters by around 100% compared to the control device.

Energy harvesting performance was then investigated under

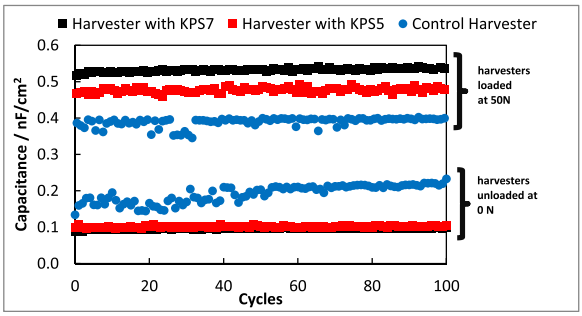

Fig. 4. Capacitance change of harvesters with and without polyHIPE springs under cyclic load from 0 to 50 N. For each cycle all the harvesters had an initial capacitance of 0.1 nF/cm^2.

simulated service conditions. For instance, considering a harvester embedded in a shoe sole, which evens out the force distribution provided by the foot impact during walking, we assume an average load of 30 N. The harvesters with an applied bias of 50 V were, therefore, cyclically compressed in a DMA from 0 to 30 N at a frequency of 2 Hz. During 10 min simulated loading cycles, the demonstration energy harvesters containing KPS7 and KPS5 units charged the storage capacitor to average voltages of 64 V and 58 V (Fig. 5), respectively, corresponding to power densities of 0.58 μW/cm^2 and 0.48 μW/cm^2, while the control energy harvester charged the storage capacitor to a voltage of 11 V, corresponding to a power density of only 0.02 μW/cm^2. The difference in the power density of the energy harvesters proves the usefulness of integrated polyHIPE springs, especially when the harvesters are operated at a high loading frequency. During high frequency loading and unloading, only a short time interval is available to allow for full separation of the silicone rubber electrode from the dielectric. Without assistance of polyHIPE spring elements, the silicone electrode does not completely detach from the dielectric upon unloading; hence, the control harvester has a higher capacitance at rest in the unloaded state as well as a lower capacitance under 30 N load. The power density of our energy harvesters with integrated foam spring elements was comparable to that reported for some other variable capacitor energy harvesters [38, 39]. To allow for comprehensive comparison, we calculated the figure of merit (FOM) using the method suggested by Basset et al. [9] of our energy harvester comprising KPS7 to be 11.6 [10^8 μW/(mm^2 Hz V^2)]. The FOM of our harvester is comparable with electrostatic energy harvesters as reviewed by Basset et al. [9], and those calculated from data reported in the review by Khan et al. [40], who reported FOM values in a range of 1–10 but much lower than the FOM of REWOD harvesters, which can be in the order of 10^6 [10^8 μW/ (mm^2 Hz V^2)] [19].

As a further illustration, the energy stored in the storage capacitor during each 10 min cycling experiment was subsequently discharged through a resistor (Figure S3, ESI), allowing the available current to be measured directly. The harvesters containing polyHIPE springs created a current flow of about 220 nA, which was 5 times higher than the control harvester. These 10 min cycles were then repeated for up to 3 h to check for stability and consistency (Fig. 5b); the current produced by the demonstration energy harvesters increased in the beginning of the test (e.g. 10–20 min) then remained constant over this time. This operating stability over reasonable timeframes (corresponding to 21600 loading cycles) indicates the mechanical robustness of the polyHIPE spring elements, and highlights the potential usefulness of our harvester concept.

Conclusions

Variable capacitive energy harvesters were developed that exploit a variable contact area between conducting silicone rubber and a printable SBTO dielectric. Crucially, polyHIPE-based spring elements were found to provide an order of magnitude improvement in harvester performance. HIPE templates were printed and polymerised onto copper Kapton® films to produce patterned macroporous springs with a height ranging from 120 μm to 330 μm. The resulting polyHIPE spring elements were subsequently coated with a conducting silicone rubber layer that conformed to the wetting cylinder shape of the spring elements. This soft, wavy electrode surface is effective for harvesting as it readily deforms under modest loads increasing the area of the silicone electrode in contact with the high dielectric constant layer, providing a large change in capacitance. Increasing the size and number of the integrated polyHIPE springs resulted in an increased capacitance change of the energy harvesters under applied cyclic load. Under a testing cyclic load of 30 N at a frequency of 2 Hz, simulating a stepping frequency during jogging, the harvesters with polyHIPE springs had a power density of 0.58 μW/cm^2, which was 25 times higher energy harvesting than the control harvesters without integrated spring elements. Furthermore, the energy harvesters exhibited a constant harvesting behaviour for a minimum constant operation time of 3 h, indicating the structural robustness of the macroporous springs.

CRediT authorship contribution statement

Victor Burre: Investigation, Formal analysis, Data curation. **Hannah Leese:** Writing – original draft, Resources, Methodology, Investigation. **Qixiang Jiang:** Writing – original draft, Supervision, Methodology, Investigation, Formal analysis, Data curation, Conceptualization. **Veronika Otáhalová:** Investigation, Formal analysis, Data curation. **Angelika Menner:** Writing – review & editing, Supervision, Conceptualization. **Alexander Bismarck:** Writing – review & editing, Supervision, Resources, Funding acquisition, Conceptualization. **Milo Shaffer:** Writing – review & editing, Supervision, Funding acquisition,

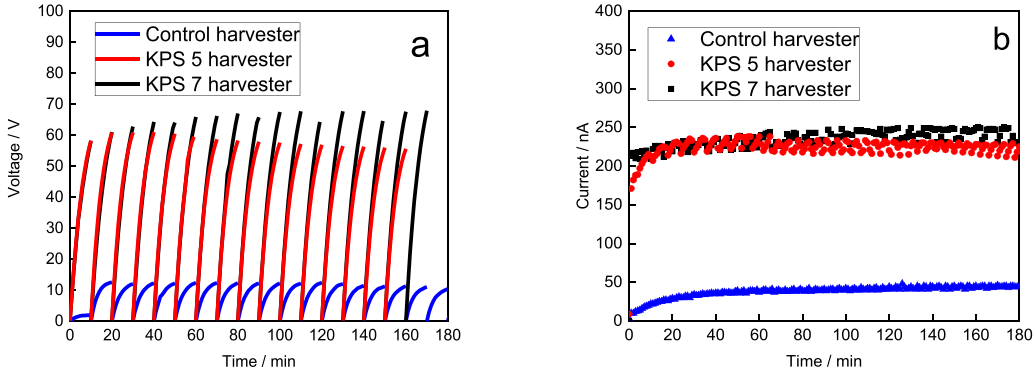

Fig. 5. Performance of energy harvesters with and without incorporated polyHIPE springs under cyclic load of 30 N operated at a loading frequency of 2 Hz. Using the energy from the harvesters to charge a storage capacitor of 1 μF and measuring the voltage increase repeatedly for 10 min (a). The produced energy by the harvesters was consumed by a 2 MΩ resistor and the current flow was monitored (b).

Conceptualization. **Robert Hahn:** Writing – review & editing, Resources, Project administration, Funding acquisition, Conceptualization.

Declaration of Competing Interest

The authors declare that they have no known competing financial interests or personal relationships that could have appeared to influence the work reported in this paper.

Data Availability

Data will be made available on request.

Acknowledgement

The authors acknowledge the EU FP7 funding through MATFLEXEND (grant number 604093) and Erasmus supporting VO for her research stay at University of Vienna. We are grateful to Nesrine Battoul Debabèche (UniVie) for her help and ingenuity to take videos of energy harvesters while loading in compression.

Appendix A. Supporting information

Supplementary data associated with this article can be found in the online version at doi:10.1016/j.nanoen.2024.109460.

References

[1] H. Li, C. Tian, Z.D. Deng, Energy harvesting from low frequency applications using piezoelectric materials, Appl. Phys. Rev. 1 (2014) 041301.
[2] Y. Tan, Y. Dong, X. Wang, Review of MEMS electromagnetic vibration energy harvester, J. Micro Syst. 26 (2017) 1–16.
[3] L. Zuo, B. Scully, J. Shestani, Y. Zhou, Design and characterization of an electromagnetic energy harvester for vehicle suspensions, Smart Mater. Struct. 19 (2010) 045003.
[4] B. Yang, C. Lee, W.L. Kee, S.P. Lim, Hybrid Energy Harvester Based on Piezoelectric and Electromagnetic Mechanisms, Journal of Micro/Nanolithography, MEMS, and MOEMS, 9 (2010) 023002.
[5] S. Boisseau, G. Despesse, B.A. Seddik, Electrostatic Conversion for Vibration Energy Harvesting, Small-scale energy harvesting, in Small-Scale Energy Harvesting, Ed. M. Lallart, Intechopen.com, 2012.
[6] A. Ali, H. Shaukat, S. Bibi, W.A. Altabey, M. Noori, S.A. Kouritem, Recent progress in energy harvesting systems for wearable technology, Energy Strategy Rev. 49 (2023) 101124.
[7] U. Jamil, R.I. Shakoor, Electrostatic energy harvester design using in-plane gap closing and in-plane overlap varying mechanisms, Int. Conf. Robot. Autom. Ind. 2019 (2019) 1–5.
[8] F. Wang, O. Hansen, Electrostatic energy harvesting device with out-of-the-plane gap closing scheme, Sens. Actuators A Phys. 211 (2014) 131–137.
[9] P. Basset, D. Galayko, A. Mahmood Paracha, F. Marty, A. Dudka, T. Bourouina, A batch-fabricated and electret-free silicon electrostatic vibration energy harvester, J. Micromech. Microeng. 19 (2009) 115025.
[10] A.C.M. de Queiroz, N.A.T. de Menezes, Energy harvesting with pairs of variable capacitors without control circuits, Analog Integr. Circuits Signal Process. 97 (2018) 533–544.
[11] T. Krupenkin, J.A. Taylor, Reverse electrowetting as a new approach to high-power energy harvesting, Nat. Commun. 2 (2011) 448.
[12] V. Vallem, E. Roosa, T. Ledinh, W. Jung, T.I. Kim, S. Rashid-Nadimi, A. Kiani, M. D. Dickey, A. Soft, Variable-Area Electrical-Double-Layer Energy Harvester, Adv. Mater. 33 (2021).
[13] R. Hahn, Y. Yang, U. Maaß, L. Georgi, J. Bauer, K.-D. Lang, Variable capacitor energy harvesting based on polymer dielectric and composite electrode, Energy Harvest. Syst. 3 (2016) 277–285.
[14] Q. Jiang, H. Barkan, A. Menner, A. Bismarck, Micropatterned, macroporous polymer springs for capacitive energy harvesters, Polymer 126 (2017) 419–424.
[15] J. Moon, J. Jeong, D. Lee, H.K. Pak, Electrical power generation by mechanically modulating electrical double layers, Nat. Commun. 4 (2013) 1487.
[16] P.R. Adhikari, N.T. Tasneem, R.C. Reid, I. Mahbub, Electrode and electrolyte configurations for low frequency motion energy harvesting based on reverse electrowetting, Sci. Rep. 11 (2021) 5030.
[17] W. Kong, P. Cao, X. He, L. Yu, X. Ma, Y. He, L. Lu, X. Zhang, Y. Deng, Ionic liquid based vibrational energy harvester by periodically squeezing the liquid bridge, RSC Adv. 4 (2014) 19356–19361.
[18] G. Carraro, S. Passaglia, G. Paolini, G. Bracco, L. Savio, G. Luciano, L. Vattuone, R. Masini, M. Smerieri, REWoD-based vibrational energy harvesting exploiting saline-solutions loaded PAAm hydrogels on micro-structured aluminium oxides electrodes, Appl. Surf. Sci. 611 (2023) 155522.
[19] H. Yang, S. Hong, B. Koo, D. Lee, Y.-B. Kim, High-performance reverse electrowetting energy harvesting using atomic-layer-deposited dielectric film, Nano Energy 31 (2017) 450–455.
[20] R. Pelrine, R. Kornbluh, J. Eckerle, P. Jeuck, S. Oh, Q. Pei, S. Stanford, Dielectric Elastomers: Generator Mode Fundamentals and Applications." Smart Structures and Materials 2001: Electroactive Polymer Actuators and Devices. Vol. 4329. SPIE, 2001.
[21] C. Bolzmacher, J. Biggs, M. Srinivasan, Flexible dielectric elastomer actuators for wearable human-machine interfaces." Smart Structures and Materials 2006: Electroactive Polymer Actuators and Devices (EAPAD). Vol. 6168. SPIE, 2006.
[22] R. Pelrine, R. Kornbluh, Q. Pei, S. Stanford, S. Oh, J. Eckerle, R. Full, M. Rosenthal, K. Meijer, Dielectric Elastomer Artificial Muscle Actuators: toward Biomimetic Motion. Smart Structures and Materials 2002: Electroactive Polymer Actuators And devices (EAPAD). Vol. 4695. SPIE, 2002.
[23] S. Rosset, H.R. Shea, Flexible and stretchable electrodes for dielectric elastomer actuators, Appl. Phys. A 110 (2013) 281–307.
[24] P. Brochu, H. Stoyanov, R. Chang, X. Niu, W. Hu, Q. Pei, Capacitive energy harvesting using highly stretchable silicone–carbon nanotube composite electrodes, Adv. Energy Mater. 4 (2014) 1300659.
[25] T. Jiang, Y. Yao, L. Xu, L. Zhang, T. Xiao, Z.L. Wang, Spring-assisted triboelectric nanogenerator for efficiently harvesting water wave energy, Nano Energy 31 (2017) 560–567.
[26] J. Chen, Z.L. Wang, Reviving vibration energy harvesting and self-powered sensing by a triboelectric nanogenerator, Joule 1 (2017) 480–521.
[27] M.S.U. Rasel, J.-Y. Park, A sandpaper assisted micro-structured polydimethylsiloxane fabrication for human skin based triboelectric energy harvesting application, Appl. Energy 206 (2017) 150–158.
[28] Y. Chiu, S.H. Wu, Flexible electret energy harvesters with parylene electret on PDMS substrates, J. Phys. Conf. Ser. 476 (2013) 012037.
[29] Y. Shao, C. Luo, B.W. Deng, B. Yin, M.-b . Yang, Flexible porous silicone rubber-nanofiber nanocomposites generated by supercritical carbon dioxide foaming for harvesting mechanical energy, Nano Energy 67 (2020) 104290.
[30] H. Zhang, Y. Lu, A. Ghaffarinejad, P. Basset, Progressive contact-separate triboelectric nanogenerator based on conductive polyurethane foam regulated with a Bennet doubler conditioning circuit, Nano Energy 51 (2018) 10–18.
[31] N.R. Cameron, High internal phase emulsion templating as a route to well-defined porous polymers, Polymer 46 (2005) 1439–1449.
[32] H.S. Leese, M. Tejkl, L. Vilar, L. Georgi, H.C. Yau, N. Rubio, E. Reixach, J. Buk, Q. Jiang, A. Bismarck, R. Hahn, M.S.P. Shaffer, High-k dielectric screen-printed inks for mechanical energy harvesting devices, Mater. Adv. 3 (2022) 1780–1790.
[33] D. Galayko, A. Dudka, A. Karami, E. O'Riordan, E. Blokhina; O. Feely, P. Basset Capacitive Energy Conversion With Circuits Implementing a Rectangular Charge-Voltage Cycle—Part 1: Analysis of the Electrical Domain, in IEEE Transactions on Circuits and Systems I: Regular *Papers*, 62 (2015) 2652-2663.
[34] M. Valkova, S. Nguyen, E. Senokos, S. Razavi, A.R.J. Kucernak, D.B. Anthony, M.S. P. Shaffer, E.S. Greenhalgh, Current collector design strategies: the route to realising scale-up of structural power composites, Compos. Sci. Technol. 236 (2023) 109978.
[35] C.F. Welch, G.D. Rose, D. Malotky, S.T. Eckersley, Rheology of high internal phase emulsions, Langmuir 22 (2006) 1544–1550.
[36] R. Wu, A. Menner, A. Bismarck, Macroporous polymers made from medium internal phase emulsion templates: effect of emulsion formulation on the pore structure of polyMIPEs, Polymer 54 (2013) 5511–5517.
[37] L. Yao, Z. Pan, J. Zhai, G. Zhang, Z. Liu, Y. Liu, High-energy-density with polymer nanocomposites containing of SrTiO3 nanofibers for capacitor application, Compos. A 109 (2018) 48–54.
[38] V. Vallem, E. Roosa, T. Ledinh, W. Jung, T.I. Kim, S. Rashid-Nadimi, A. Kiani, M. D. Dickey, A. Soft, Variable-area electrical-double-layer energy harvester, Adv. Mater. 33 (2021) 2103142.
[39] L. Bu, H.Y. Xu, B.J. Xu, L. Song, Micro-fabricated liquid encapsulated energy harvester with polymer barrier layer as liquid electret interface, J. Phys. Conf. Ser. 557 (2014) 012036.
[40] F.U. Khan, M.U. Qadir, J. Micromech. Microeng. 26 (2016) 103001.